Electronic Supplementary Material (ESI) for RSC Advances.

Supporting Information

Hydrogen titanate constructed by ultrafine nanobelts as advanced anode materials with high-rate and ultra-long life for lithium-ion batteries

Qinghua Tian, Yang Tian, Zhengxi Zhang,* Li Yang* and Shin-ichi Hirano

[a]School of Chemistry and Chemical Engineering, Shanghai Jiao Tong University, Shanghai 200240, P. R. China

[b]Hirano Institute for Materials Innovation, Shanghai Jiao Tong University, Shanghai 200240, P. R. China

*Corresponding author e-mail address: liyangce@sjtu.edu.cn (L. Yang), zhengxizhang@sjtu.edu.cn (Z. X. Zhang)

Tel: +86 21 54748917, Fax: +86 21 54741297

* Corresponding author. Tel.: +86 21 54748917; fax: +86 21 54741297. E-mail address: liyangce@sjtu.edu.cn (L. Yang), zhengxizhang@sjtu.edu.cn (Z.X. Zhang).

Fig. S1 shows the SEM images of different $H_2Ti_3O_7$ samples obtained from sodium hydroxide (NaOH) concentration--dependent experiment (other conditions kept unchanged, such as the hydrothermal temperature and hydrothermal time were fixed at 180 ^oC and 48 h, respectively). The sample collected at 6.25 M of NaOH has morphology of irregular micro/nanoparticles constructed by nanoneedles units, as shown in Fig. S1 (a1, a2). When the NaOH concentration increased to 7.5 M, the edges of obtained micro/nanoparticles become smooth and the building units transform into intertwined seeming nanowires, as well as the distinct interspaces in particles are clearly seen as displayed in Fig. S1 (b1, b2). When the NaOH concentration further increased to 10 M, however, the micro/nanoparticles disappear, instead, the monodispersed nanobelts with a broader width of several hundred nm and a length of several um are observed as showed in Fig. S1 (c1, c2). Followed by the temperature-dependent experiment (other conditions kept unchanged, such as the NaOH concentration and hydrothermal time were fixed at 7.5 M and 48 h, respectively) were also carried out to investigate the influence of hydrothermal temperature on the morphology of $H_2Ti_3O_7$ samples, the SEM images of obtained samples as showed in Fig. S2. When the temperature selected at 150 ^oC, the prepared sample is composed of nanoparticles with a size of near 1 um, and the particles are seemingly assembled by smaller primary units as displayed in Fig. S2 (a1, a2). After the temperature increased to 200 ^oC, the morphology of collected sample becomes monodispersed broader nanobelts, which is similar with NaOH concentration-dependent experiment at 10 M except the length became longer, as shown in Fig. S2 (b1, b2). Thus, the NaOH concentration and hydrothermal temperature play important roles in the morphology-engineered of $H_2Ti_3O_7$ samples.

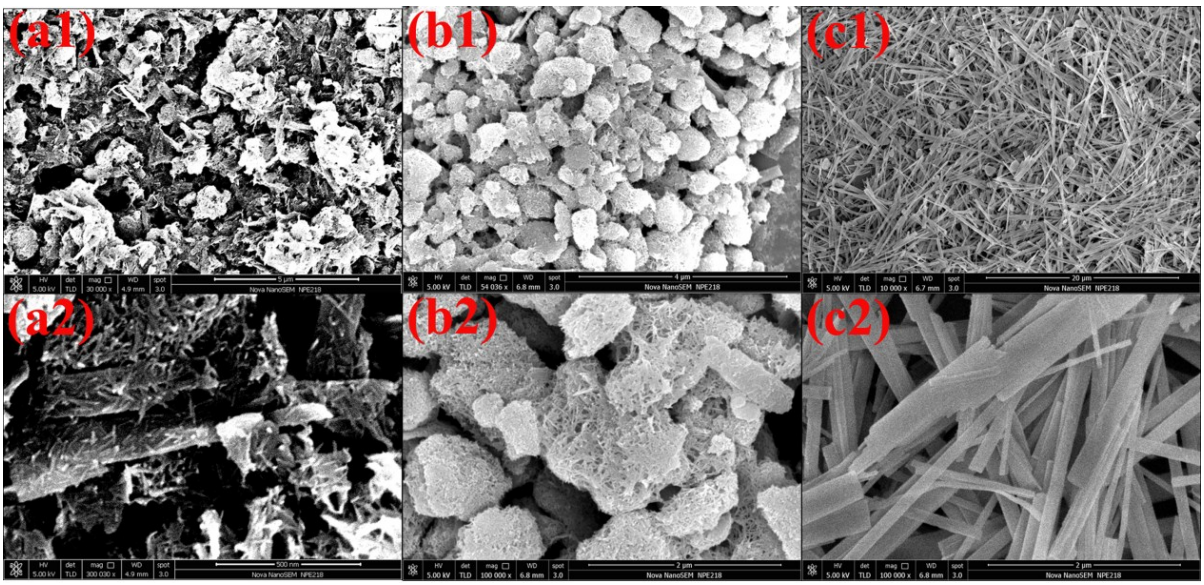

Fig. S1 SEM images of samples prepared at different NaOH concentration: (a1, a2) 6.25 M; (b1, b2) 7.5 M; (c1, c2) 10 M.

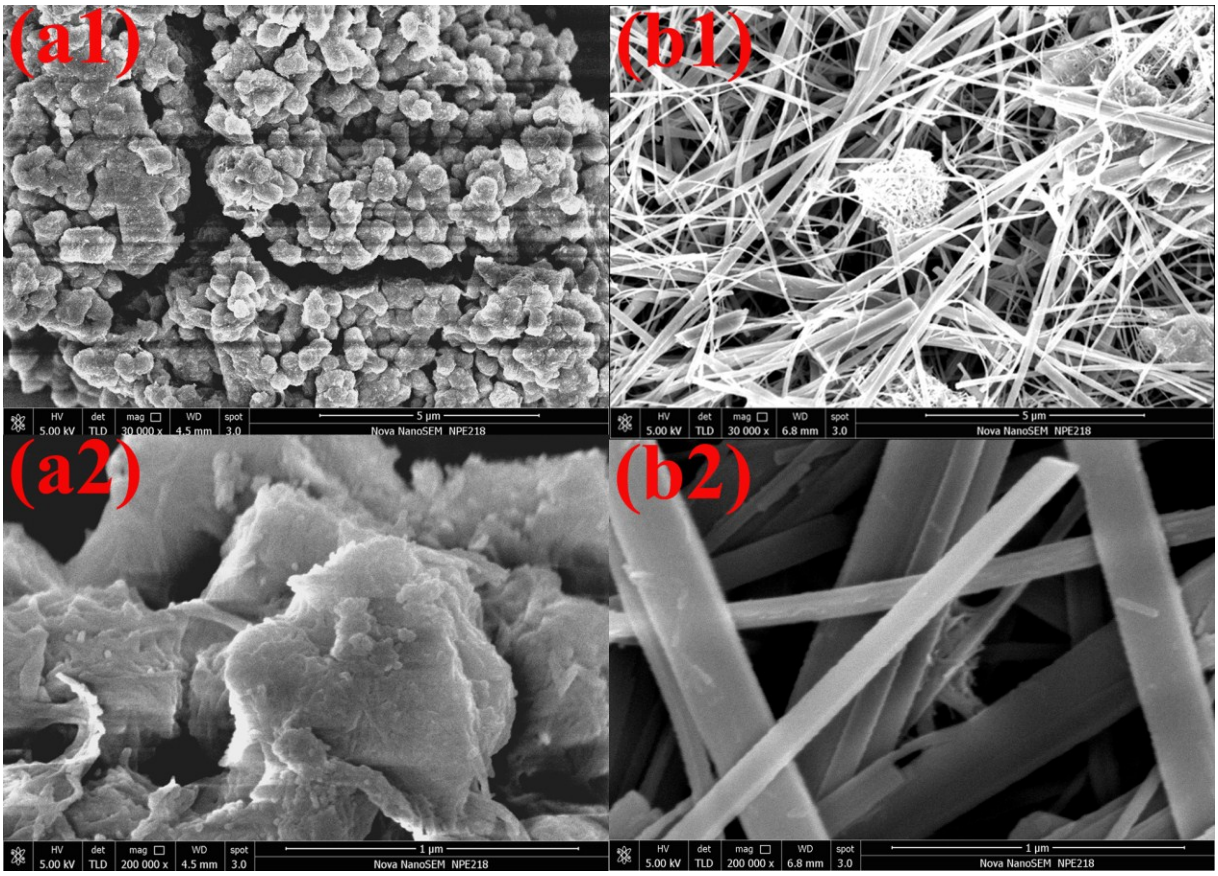

Fig. S2 SEM images of samples prepared at hydrothermal temperature: (a1, a2) 150 ^{o}C; (b1, b2) 200 ^{o}C.

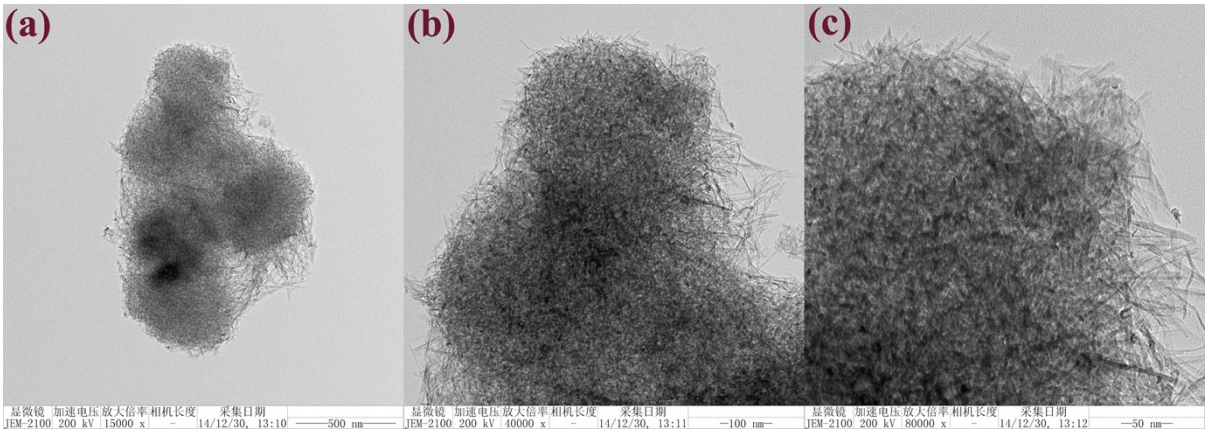

Fig. S3 TEM images with different magnifications of $H_2Ti_3O_7$ with a unique morphology of smooth micro/nanoparticles constructed by intertwined ultrafine nanobelts.

Fig. S4 and S5 give the TEM images of samples obtained from the $H_2Ti_3O_7$ heating treatment at different temperatures. When the calcination is performed below 400 ^oC, the samples remain the same morphology of $H_2Ti_3O_7$ (Fig. S3). But, the sample gained from $H_2Ti_3O_7$ calcination at 400 ^oC, as shown in Fig. S5(a1, a2), has a changed morphology compared to $H_2Ti_3O_7$, some nanobelts units collapse into nanorods or particles, and the micro/nanoparticles become compact. After the calcination temperature is further increased to 500 ^oC (Fig. S5 (b1, b2)) or 600 ^oC (Fig. S5 (c1, c2)), the nanobelts units are almost all broken and become into shortened nanorods or nanoparticles, as well as the micro/nanoparticles become more compact. The insets in each TEM image are the SAED patterns indicating the crystallinity of samples increases with the calcination temperature increases.

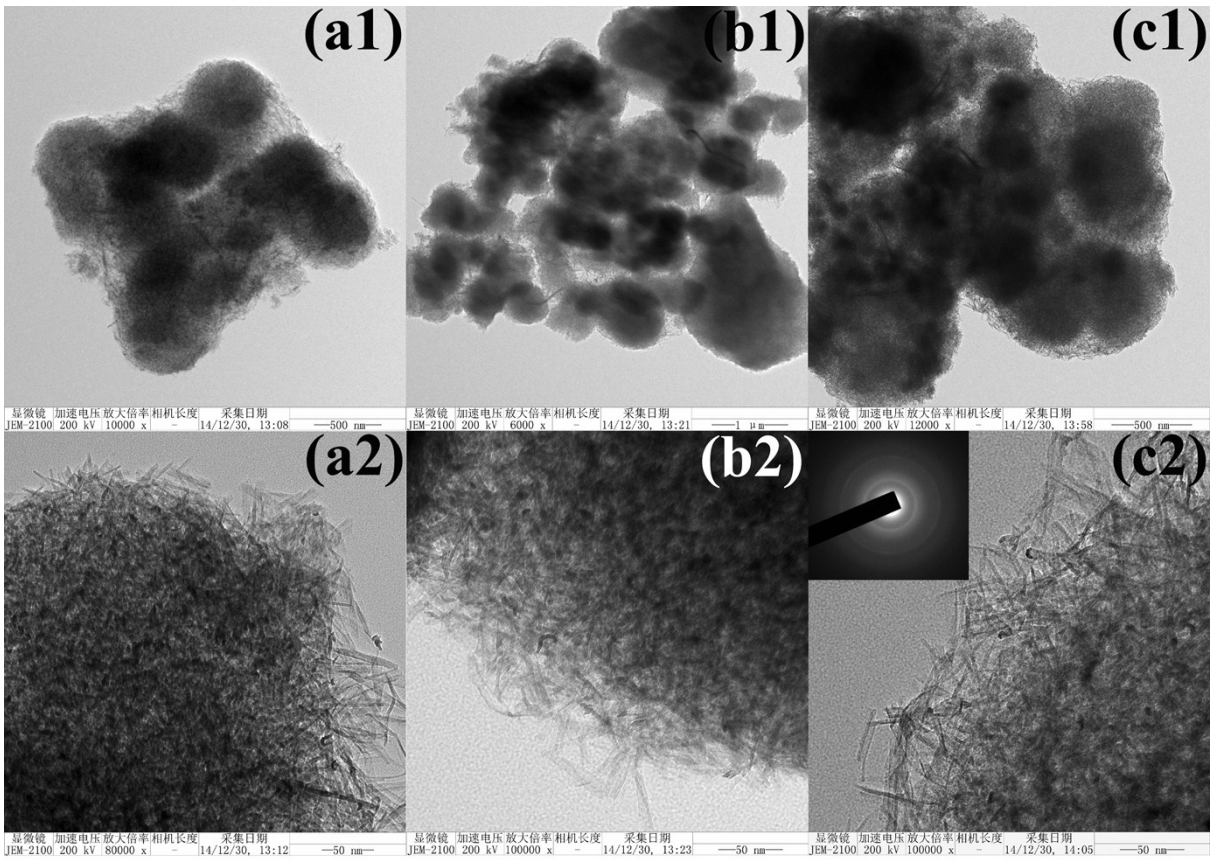

Fig. S4 TEM images of samples obtained from $H_2Ti_3O_7$ calciantion at different temperatures under air: (a1, a2) 0 ^oC (no heating treatment); (b1, b2) 200 ^oC; (c1, c2) 300 ^oC.

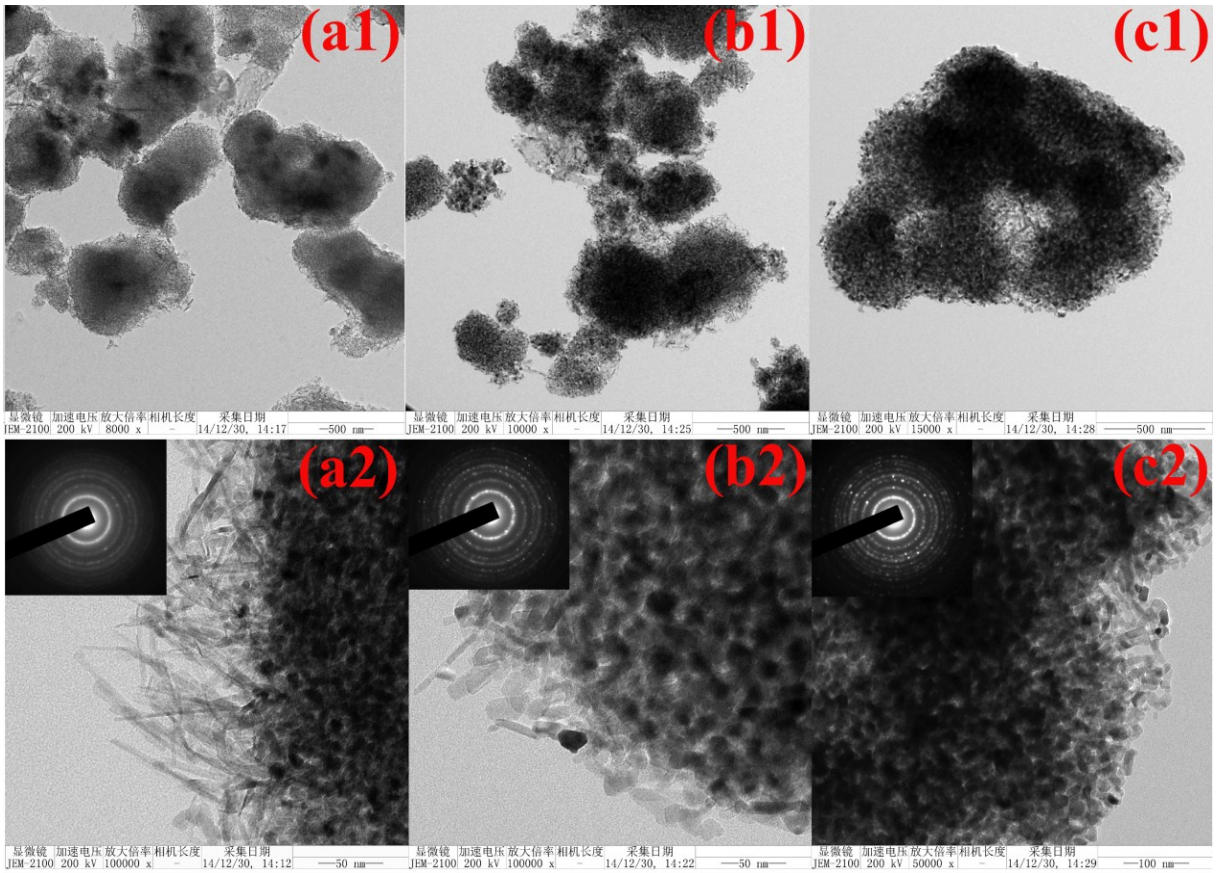

Fig. S5 TEM images of samples obtained from $H_2Ti_3O_7$ calciantion at different temperatures under air: (a1, a2) 400 ^oC; (b1, b2) 500 ^oC; (c1, c2) 600 ^oC.

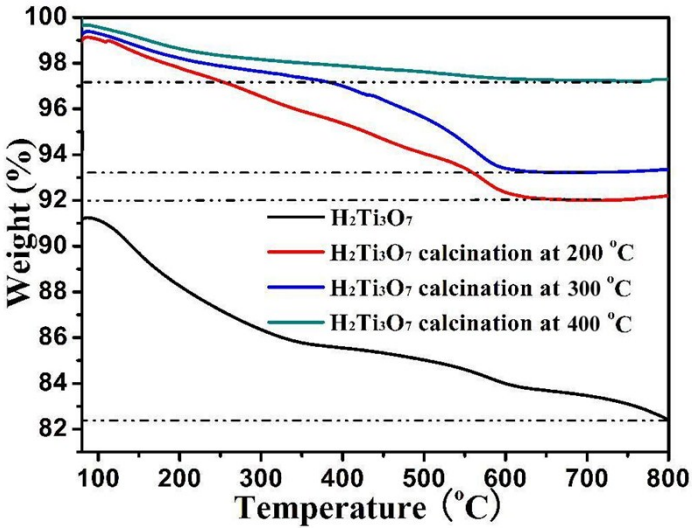

Fig. S6 The TGA of different samples was carried out at a heating rate of 10 °C under N_2 (the temperature firstly kept at 80 °C for 2 h to removal the adsorbed water from air, then increased to 800 °C at a heating rate of 10 °C).

In Fig. S8a all samples exhibit typical type-IV adsorption isotherms with H3 hysteresis loops which are the characteristic isotherms of mesoporous materials, indicating all of them have mesoporous structures. Barrett–Joyner–Halenda (BJH) pore analysis shows an average pore size distribution ranging from 6.5-6.8 nm for the samples obtained from $H_2Ti_3O_7$ calcined at below 400 °C, while the samples obtained from $H_2Ti_3O_7$ calcined at above 300 °C have a broad pore size distribution ranging from 9.6-11.3 nm, as shown in Fig. S8c. The change of pore size distribution between $H_2Ti_3O_7$ calcined at below 400 °C and $H_2Ti_3O_7$ calcined at above 300 °C could be atttibuted to the morphologies change during heating treatment.

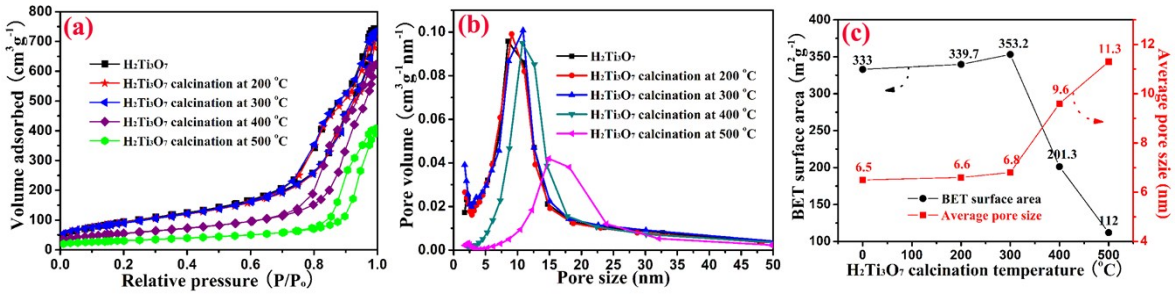

Fig. S7 (a) N_2 adsorption/desorption isotherms and (b) the corresponding pore size distribution of f different samples; (c) Plots of BET surface−calcination temperature, and Plots of average pore size−calcination temperature.

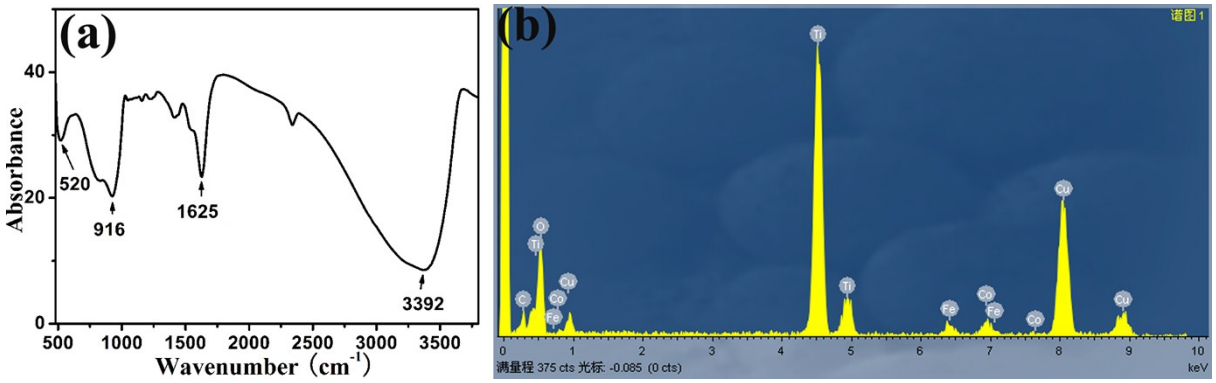

Fig. S8 (a) FTIR for the HTO-HT; (b) EDS of HTO-HT (The C, Cu, Fe and Co peaks come from micro-grid used as the sample stage in TEM measurements).

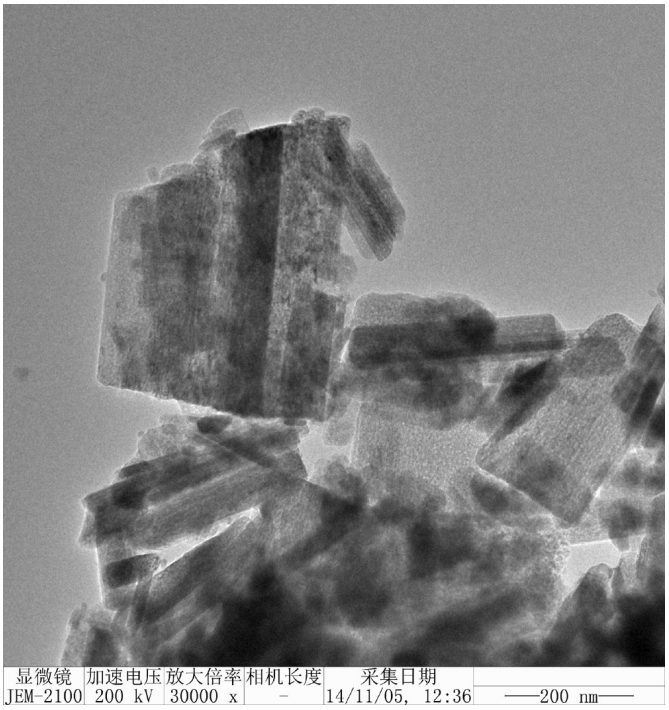

Fig. S9 TEM image of the sample (HTO-HTB) prepared by monodispersed broad $H_2Ti_3O_7$ nanobelts (Figure S2b2) calcination at 300 ^oC under air.

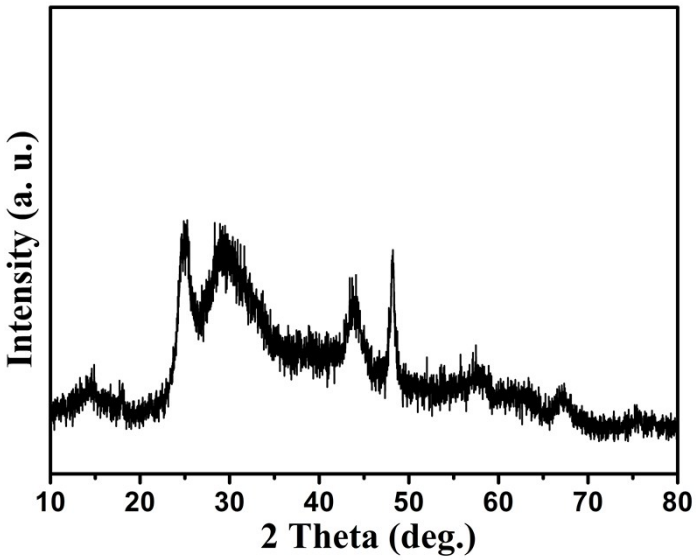

Fig. S10 XRD patterns of the HTO-HTB.

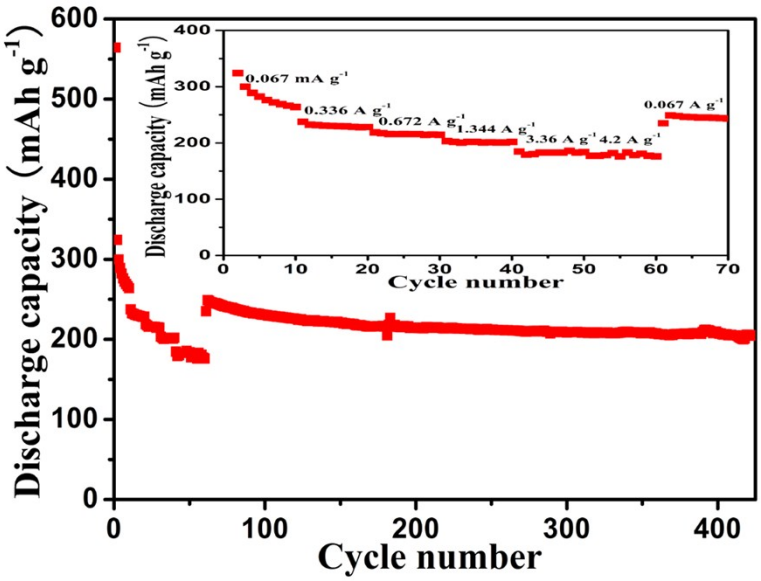

Fig. S11 Rate capability of HTO-HT.